Refractory, Ceramic, and Composite Materials
Тугоплавкие, керамические и композиционные материалы

Structural, mechanical, and tribological properties of TiC–C–Al hybrid composites fabricated by self-propagating high-temperature synthesis combined with spontaneous infiltration

E. R. Umerov[1], A. P. Amosov[1] ✉, E. I. Latukhin[1], A. D. Kachura[1],

I. A. Rastegaev[2], M. A. Afanasiev[2]

[1] Samara State Technical University
244 Molodogvardeyskaya Str., Samara 443100, Russia
[2] Togliatti State University
14 Belorusskaya Str., Tolyatti, Samara region 445020, Russia

✉ egundor@yandex.ru

Abstract. The addition of graphite particles to aluminum improves its tribological properties due to the self-lubricating effect, while reinforcement of such aluminum matrix composites (Al–C) with the ceramic phase of titanium carbide (TiC), known for its high hardness and strength, results in Al–TiC–C hybrid composites with enhanced physical and mechanical properties and improved wear resistance. This study explores a novel energy-efficient approach to fabricating Al–TiC–C composites by combining self-propagating high-temperature synthesis (SHS) of porous TiC–C composite frameworks with subsequent spontaneous infiltration using molten aluminum. The titanium carbide was synthesized from a stoichiometric powder mixture of titanium and graphite (Ti + C). To introduce free carbon, additional graphite powders with particle sizes of 10–15 and 100–1000 μm, as well as chopped carbon fibers with a diameter of 7 μm and a length of 3 mm, were added to the stoichiometric mixture. The microstructure and composition of the resulting composites were examined using scanning electron microscopy with energy-dispersive spectroscopy and X-ray diffraction analysis. Density was measured by hydrostatic weighing, while Brinell hardness, compressive strength, and tribological properties were evaluated using a pin-on-disk tribometer. It was found that fine graphite particles (10–15 μm) dissolved almost completely in molten aluminum, whereas coarse graphite (100–1000 μm) and carbon fibers remained intact. The compressive strength of the carbon-containing aluminum matrix composites ranged from 203 to 233 MPa. Under dry sliding conditions, abrasive wear was the predominant wear mechanism, accompanied by a high coefficient of friction (0.88–0.98); however, the wear rate of the composite containing coarse graphite was three times lower.

Keywords: composite material, aluminum, titanium carbide, graphite, self-propagating high-temperature synthesis (SHS), porous framework, infiltration, tribology

PM & FC

POWDER METALLURGY AND FUNCTIONAL COATINGS. 2025;19(2):24–38
Umerov E.R., Amosov A.P., and etc. Structural, mechanical, and tribological properties of TiC–C–Al ...

Структурные, механические и трибологические особенности гибридных композитов TiC–C–Al, изготовленных методом самораспространяющегося высокотемпературного синтеза в сочетании с самопроизвольной инфильтрацией

Э. Р. Умеров[1], А. П. Амосов[1] ✉, Е. И. Латухин[1], А. Д. Качура[1],
И. А. Растегаев[2], М. А. Афанасьев[2]

[1] **Самарский государственный технический университет**
Россия, 443100, г. Самара, ул. Молодогвардейская, 244
[2] **Тольяттинский государственный университет**
Россия, 445020, Самарская обл., г. Тольятти, ул. Белорусская, 14

✉ egundor@yandex.ru

Аннотация. Добавление частиц графита к алюминию позволяет улучшить его трибологические свойства за счет проявления эффекта самосмазывания, а армирование таких алюмоматричных композитов (Al–C) керамической фазой карбида титана (TiC) с высокими твердостью и прочностью – получить гибридные композиты Al–TiC–C с повышенными физико-механическими свойствами и улучшенной износостойкостью. В настоящей работе рассмотрено применение нового энергоэффективного подхода к получению композитов Al–TiC–C путем сочетания метода самораспространяющегося высокотемпературного синтеза (СВС) пористых композиционных каркасов из карбида титана и свободного углерода (TiC–C) с последующей инфильтрацией их расплавом алюминия. Для синтеза карбида титана использовалась стехиометрическая смесь порошков титана и графита Ti + C, а для получения свободного углерода в эту стехиометрическую смесь добавлялись порошки графита с размерами частиц 10–15 и 100–1000 мкм, а также рубленое углеволокно диаметром 7 мкм и длиной 3 мм. Для изучения микроструктуры и состава новых композитов использовались методы сканирующей электронной микроскопии с энергодисперсионной спектрометрией и рентгенофазового анализа. Также определены плотность гидростатическим взвешиванием, твердость по Бринеллю, прочность при сжатии и трибологические свойства на трибометре по схеме «*pin–on–disk*». Установлено, что добавляемый графит с мелкими частицами (10–15 мкм) практически полностью растворяется в расплаве алюминия, а крупнозернистый графит (100–1000 мкм) и углеволокно в нем сохраняются. Предел прочности при сжатии углеродсодержащих алюмоматричных композитов составил 203–233 МПа. Установлено, что при сухом трении реализуется преимущественно абразивный механизм изнашивания с высоким коэффицентом трения (0,88–0,98), но в 3 раза меньшим износом образца композита, полученного с добавлением крупнозернистого графита.

Ключевые слова: композиционный материал (КМ), алюминий, карбид титана, графит, самораспространяющийся высокотемпературный синтез (СВС), пористый каркас, инфильтрация, трибология

Introduction

Aluminum matrix composites (AMCs) reinforced with graphite and ceramic particles are considered promising materials for tribological applications [1–3]. Graphite, classified as a solid lubricant, imparts self-lubricating properties to the strengthened matrix, resulting in reduced friction coefficients and prevention of seizure, thus making aluminum-based materials suitable for tribotechnical applications. The aluminum – graphite composite was first successfully fabricated in 1969. Over the past 50 years, several

successful tests have demonstrated the use of aluminum–graphite pistons, bearings, and connecting rods in both gasoline and diesel engines. For example, aluminum–graphite cylinder liners exhibited improved performance (without scuffing) against aluminum pistons in Alpha Romeo and Ferrari Formula 1 racing cars [4]. The main challenge in fabricating graphite-containing AMCs lies in the poor wettability of carbon-based materials by molten aluminum at temperatures below 1320 K, which hinders good interfacial adhesion and uniform distribution of graphite particles throughout the matrix. Another commonly used approach

ПМ и ФП
ИЗВЕСТИЯ ВУЗОВ

ИЗВЕСТИЯ ВУЗОВ. ПОРОШКОВАЯ МЕТАЛЛУРГИЯ И ФУНКЦИОНАЛЬНЫЕ ПОКРЫТИЯ. 2025;19(2):24–38
Умеров Э.Р., Амосов А.П. и др. Структурные, механические и трибологические особенности гибридных ...

to strengthen aluminum alloys is reinforcement with carbon fibers (CFs) [5].

Powder metallurgy and casting technologies are the most widespread methods for producing metal matrix composites, as they can provide acceptable levels of density, porosity, mechanical and tribological properties under industrial conditions at a reasonable cost [6; 7]. Powder metallurgy methods are based on processing materials in the solid state and may include such operations as mixing, pressing, and sintering to achieve minimal porosity in the resulting composite. Among these methods, self-propagating high-temperature synthesis (SHS) stands out as a technique that enables the synthesis of various ceramic phases from elemental powders through an exothermic chemical reaction. The heat released during the SHS reaction results in a high temperature of the synthesized ceramic product [8]. In addition, the rapid reaction is accompanied by intensive gas evolution, which leads to the formation of an open porous capillary structure with pore sizes ranging from 0.1 μm to 1–2 mm, depending on the synthesis conditions and the composition of the initial powders [9; 10].

Liquid-phase methods include stir casting, infiltration under pressure, and spontaneous (pressureless) infiltration [11; 12]. For instance, a carbon – graphite – aluminum composite was produced by infiltrating a porous (14–16 %) carbon – graphite framework with molten AK12 alloy at temperatures up to 700 °C and pressures up to 5 MPa [13]. However, improving wettability and limiting interfacial reactions required multiple process steps, including pre-coating the carbon – graphite pore surfaces with nickel sulfate, vibro-vacuum treatment before infiltration, and mechanical densification of the composite to reduce residual porosity after aluminum infiltration, which significantly complicated the process. In [14], it was shown that infiltration at 0.8 MPa, 1073 K, and a 60 s holding time in an argon atmosphere enables the fabrication of an aluminum – carbon fiber composite. However, a substantial amount of the undesirable Al_4C_3 phase formed as a result of their interaction.

The main drawback of aluminum matrix composites with graphite as a filler is their relatively low strength. To improve this property, an additional strengthening component is introduced – for example, a metal oxide or carbide with high hardness and strength. One of the most promising candidates is titanium carbide (TiC), which has a hardness of 20–25 GPa and is frequently considered as a reinforcement for aluminum and its alloys. AMCs reinforced with TiC particles exhibit superior mechanical strength, which is also attributed to the stronger interfacial bonding in the Al–TiC system compared to composites reinforced with SiC particles. The work of adhesion between TiC and aluminum increases from 1317 to 1608 mJ/m^2 as the reaction temperature rises from 800 to 1000 °C [15]. Aluminum matrix composites reinforced with TiC particles also demonstrate enhanced tribological performance, comparable to that of conventional aluminum-based tribological alloys such as AO20-1 and bronzes under dry sliding conditions at contact pressures up to 0.7 MPa. Furthermore, under dry sliding against 40Kh steel, the aluminum alloy AK12M2MgN with up to 10 % TiC[1] shows a reduced coefficient of friction, regardless of the applied pressure [16].

To achieve optimal tribological performance, the development of poly-reinforced (hybrid) composites has been proposed. These contain both a hard, high-strength carbide and self-lubricating graphite (Gr). Aluminum matrix composites such as A356–10 % SiC–4 % Gr and A356–5 % Al_2O_3–3 % Gr have been developed for use in cylinder liners of cast aluminum engine blocks. Under dry friction conditions, these composites formed graphite-based tribofilms that improved the wear resistance of aluminum and reduced the coefficient of friction [17]. Hybrid composites based on aluminum and its alloys – such as 2024–5 % SiC–x % Gr ($x = 0$, 5 and 10) [18] and 7075–Gr [19] – have also been fabricated via powder metallurgy and exhibited excellent tribological performance due to the self-lubricating effect. In [20], it was shown that the combined reinforcement of 7075 aluminum alloy with TiC particles (5–15 %) and graphite (3–5 %) significantly improved the material's tribological properties, reducing both wear and the coefficient of friction under dry sliding conditions.

The authors of [21] note that 5 % of TiC nanoparticles and up to 10 % of graphite not only reduced the wear rate and coefficient of friction of aluminum but also promoted the formation of a stable lubricating layer under long sliding distances and high sliding speeds. This layer consisted of a stable graphite – TiC composition on the contact surface. Typically, ceramic – metal composites with self-lubricating properties are fabricated by powder metallurgy, which involves prolonged high-temperature sintering in a protective atmosphere. This significantly complicates the production process and increases its cost.

A more economically feasible alternative may be spontaneous infiltration, a simple and low-cost method based on the capillary action of liquid metal into a porous body. This process does not require special equipment to create pressure or maintain a gas atmosphere. However, the key prerequisite for implementing this method is achieving good wettabi-

---

[1] Here and hereinafter, wt. % is implied unless otherwise specified.

PM & FC

POWDER METALLURGY AND FUNCTIONAL COATINGS. 2025;19(2):24–38
Umerov E.R., Amosov A.P., and etc. Structural, mechanical, and tribological properties of TiC–C–Al ...

lity of the porous solid by the molten metal, which is often unachievable in industrial settings due to the different natures of ceramics and metals. In this study, the authors propose a new energy-efficient and simple approach for producing ceramic–metal composite materials by combining the exothermic SHS method with the self-heating of the synthesized porous ceramic (SHS framework) to temperatures exceeding 2000 °C. At such temperatures, good wettability of the ceramic by metals such as aluminum, copper, and tin can be achieved, allowing spontaneous infiltration of these melts into SHS frameworks [22–24]. A characteristic feature of such materials synthesized in air is their multiphase composition. For example, SHS-derived ceramic frameworks based on MAX phases such as Ti_3SiC_2 and Ti_3AlC_2 contain not only the target phase but also a significant amount of TiC, along with minor amounts of TiO_2, TiN, and Al_2O_3, which are poorly wetted by molten aluminum. However, the observed spontaneous infiltration of the melt into these frameworks suggests that the predominant factor enabling wettability is the extremely high temperature of the ceramic immediately after SHS [25; 26].

In the present study, a new approach is proposed for fabricating composites from a non-wettable component – carbon (graphite and carbon fiber) – by introducing it into the initial SHS mixture. In this case, excess carbon that does not participate in the synthesis reaction remains in the SHS system as an inert additive, which undergoes substantial heating during the exothermic synthesis of the ceramic compound. Thus, the aim of this work was to investigate the feasibility of producing TiC–C–Al hybrid composites by introducing excess carbon (graphite and carbon fiber) into the Ti + C reactive mixture to synthesize a porous TiC–C SHS framework followed by spontaneous infiltration with molten aluminum.

Materials and methods

The following materials were used in this study:

– titanium powder grade TPP-7 (TU 1715-449-05785388, particle size ≤ 300 μm);

– colloidal graphite grade S-2 (GOST 17022-81, particle size ≤ 15 μm) and graphite grade GMZ (TU 48-20-16-81, particle size 100–1000 μm);

– chopped carbon fiber grade SYT45S (Zhongfu Shenying Carbon Fiber Co., LTD, length 3 mm, diameter 7 μm).

Dried TPP-7 titanium and S-2 graphite powders, taken in a stoichiometric ratio for TiC synthesis via the reaction Ti + C → TiC, were pre-mixed in a ball mill at 105 rpm for 20 min. A 100 % excess of car-

bon – in the form of S-2 graphite, GMZ graphite, or chopped carbon fiber (CF) – was added at the final mixing stage to prevent particle size reduction of the graphite. The amount of the excess additive corresponded to the mass of S-2 graphite in the stoichiometric Ti + C mixture. The loose powder charges were loaded into cylindrical hollow crucibles (22 mm in diameter) made of single-layer paper and placed into a recess in the sand, into which molten aluminum was then poured after ignition of the charge. was applied to the powder charge to ignite it, i.e., to initiate the SHS process in combustion mode. The general experimental setup is shown in Fig. 1.

Four types of initial powder charge were prepared with the following compositions:

1 – Ti (TPP-7 titanium) + C (S-2 graphite);

2 – Ti (TPP-7 titanium) + C (S-2 graphite) + 100 % excess C (S-2 graphite);

3 – Ti (TPP-7 titanium) + C (S-2 graphite) + 100 % excess C (GMZ graphite);

4 – Ti (TPP-7 titanium) + C (S-2 graphite) + 100 % excess C (carbon fiber).

The total powder charge mass was 40 g without excess carbon and 48 g with excess carbonaceous additives. At the moment of ignition, molten aluminum – pre-melted in an electric furnace at 900 °C – was poured into the recess in the sand, onto the side surface of the ignited powder charge. During the SHS synthesis of titanium carbide, the high-temperature (up to 2800 °C) [10] combustion zone of the porous sample absorbed the molten aluminum. The combus-
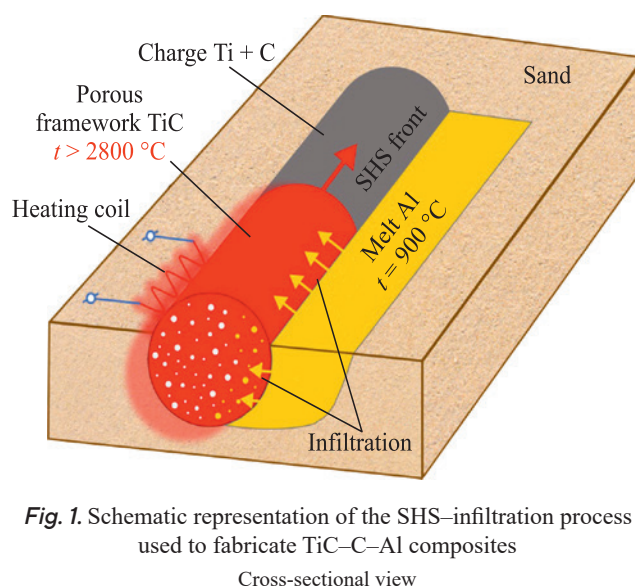

Fig. 1. Schematic representation of the SHS–infiltration process used to fabricate TiC–C–Al composites

Cross-sectional view

Рис. 1. Схема сочетания СВС и инфильтрации для получения композитов TiC–C–Al

Вид с разрезом

tion and infiltration process lasted approximately 20–25 s, after which the remaining aluminum melt was removed to facilitate subsequent mechanical processing and the fabrication of cylindrical composite samples for further testing.

Microstructure and elemental composition analyses were performed using a Tescan Vega 3 scanning electron microscope (SEM, Czech Republic) equipped with an X-act energy-dispersive spectroscopy (EDS) system. Phase composition of the synthesized products was identified by *X*-ray diffraction (XRD). XRD analysis was carried out using an automated ARL X'trA diffractometer (Thermo Scientific, Switzerland) with $\text{Cu}K_\alpha$ radiation under continuous scanning in the 2θ range of 20–80° at a rate of 2°/min. The resulting diffraction patterns were processed using the WinXRD software package (Switzerland). Experimental density was determined by hydrostatic weighing in accordance with GOST 20018–74. Porosity was calculated as the difference between the theoretical and experimental density values of the composites. Brinell hardness was measured using a 5 mm steel ball under a load of 98 N, following GOST 9012–59. Uniaxial compression tests were conducted according to the guidelines of GOST 25.503–97 using cylindrical samples with a diameter of 20.1 ± 0.1 mm and a height of 19.4 ± 0.8 mm. The tests were performed on a WDW-300E universal testing machine (Time Group, China) at a crosshead speed of 1 mm/min. Sample dimensions before and after compression were measured using a 500-205 caliper (Mitutoyo, Japan) with a precision of 0.01 mm.

Based on the test results, stress–strain curves $\sigma^c = f(\varepsilon)$ were plotted, showing the dependence of compressive stress (σ^c) on relative strain (ε), taking into account the stiffness of the testing machine in accordance with GOST 25.503–97. The materials were then evaluated using the following parameters:

• elastic characteristics – from the slope angle of the linear portion of the curve ($\text{tg}^c\alpha$) and the conventional compressive yield strength ($\sigma^c_{0.2}$);

• strength characteristics – from the compressive strength (σ^{c*}_u), where σ^{c*}_u was determined using a non-standard approach: its value was taken as the stress at the inflection point of the $\sigma^c = f(\varepsilon)$ curve observed after $\sigma^c_{0.2}$).

Tribological testing of the materials was carried out on a TRB50N tribometer (Nanovea, USA) using a rotary *pin-on-disk* configuration (ASTM G99), in which a vertically positioned cylindrical composite sample rotates about its longitudinal axis, and a friction counterbody (indenter) in the form of a stationary 6.35 mm diameter 100Cr6 steel ball is pressed against its upper face, 3 mm from the axis of rotation, under the following conditions:

– normal load on the indenter: $F = 2$ N;

– rotational speed of the sample: 200 rpm;

– wear track diameter: 6.0 mm, corresponding to a sliding speed of 62.8 mm/s;

– test duration: $\tau = 1$ h 19 min 54 s or a sliding distance of $L = 250$ m;

– lubrication regime: dry sliding.

Damage to the indenter was evaluated by measuring the wear scar diameter using the refined ASTM G99 formula. Damage to the composite sample was evaluated by 3D scanning the wear track on its end face and determining the lost metal volume (V) between the worn surface profile and a plane corresponding to the original undamaged surface. The wear scar diameter and wear volume of the sample were determined using a LEXT OLS4000 confocal laser scanning microscope (Olympus, Japan). Based on the volumetric wear data for both the samples and the indenters, the wear rate ($\dot{I}$) and wear resistance (W) were calculated using the formulas:

$$\dot{I} = \frac{V}{\tau},$$

$$W = \frac{1}{I} = \frac{L}{V},$$

where I or $\dot{I}$ is the wear rate in mm³/m or mm³/min, and L is the sliding distance in meters.

Throughout the tribological tests, the maximum (μ_{max}) and average (μ_{av}) values of the kinetic coefficient of friction were continuously measured in accordance with ASTM G40.

To assess changes related to the addition of excess carbon, two additional comparative parameters were used: the relative wear resistance (ε_I) and the friction coefficient stability (α), calculated as follows

$$\varepsilon_I = \frac{V_E}{V_C},$$

$$\alpha = \frac{\mu_{av}}{\mu_{max}},$$

where V_E and V_C are the average volumetric wear values of the reference material and the comparison material, respectively.

In this study, the baseline material was the Al–TiC composite fabricated without excess carbon. The ε_I parameter was calculated for both the test samples and the counterbody (indenter), since damage to the indenter is also a result of its interaction with the tested materials.

PM & FC

POWDER METALLURGY AND FUNCTIONAL COATINGS. 2025;19(2):24–38

Umerov E.R., Amosov A.P., and etc. Structural, mechanical, and tribological properties of TiC–C–Al ...

Results and discussion

Previous studies have shown that the least defective SHS-derived TiC frameworks were synthesized using relatively coarse titanium powder TPP-7 and graphite powder S-2 [13]. Therefore, these powder grades were chosen as the basis for studying the effect of excess carbon of various forms and particle sizes on the formation of TiC–C–Al hybrid composites. It is important to note that frameworks of all four types were successfully produced via SHS and infiltrated with molten aluminum.

As shown in Fig. 2, the composite samples after lathe machining exhibit a metallic luster and show virtually no large pores or cracks. Sample *B*, synthesized with an excess of fine S-2 graphite, is visually indistinguishable from sample *A* – the TiC–Al composite without excess carbon additives. In contrast, sample *C*, fabricated with the addition of coarse GMZ graphite (0.1–1.0 mm), shows uniformly distributed graphite particles of corresponding size throughout the entire volume. Sample *D*, synthesized with carbon fiber addition, contains dark inclusions formed by carbon fiber clusters embedded in the aluminum matrix.

The microstructure, phase composition, and porosity of the TiC–Al SHS composite have been described in detail in previous studies [27; 28]. In the sample without excess carbon, two main phases were identified: a metallic phase (Al) forming a continuous matrix that filled all accessible pore volume, and a ceramic phase (TiC) represented by tightly sintered equiaxed particles with a size of approximately 5–10 μm. The observed phase composition was as follows: 50–55 % Al, 40–45 % TiC, and up to 5 % secondary phases (Al_4C_3, $TiAl_3$, Al_2O_3). These minor phases were not detected by XRD due to their low content, but their presence was confirmed by SEM and EDS analysis. The Al_4C_3 phase appeared in the aluminum matrix as black acicular structures measuring up to 50–70 μm in length

and 5–15 μm in width, while $TiAl_3$ was also found in the Al matrix, typically surrounding TiC particles. Since both secondary phases are products of high-temperature interaction between TiC and Al, they were observed primarily at or near the ceramic – metal interface of the composite. The residual porosity of such composites was up to 6–8 %, with an average density of 3.12 g/cm³.

Fig. 3 shows the microstructure and the *X*-ray diffraction (XRD) pattern of the phase composition of the TiC–C(C-2)–Al composite, in which the excess carbon is introduced in the form of fine graphite particles approximately 15 μm in size. It can be seen that the ceramic and metallic components of the composite are tightly bonded. A few large pores are observed, while no systematic fine porosity is present, indicating good wettability. The ceramic region of the composite exhibits a gradient structure: the outer crust consists of densely sintered relatively large (20–40 μm) particles of non-stoichiometric TiC_x, beneath which there is a less compact zone composed of smaller TiC_x particles (5–15 μm) embedded in aluminum. In the central region of the ceramic, two phases are observed – Al and the intermetallic compound $TiAl_3$. It is worth noting that in an open pore within the Al matrix, where significant amounts of Al_4C_3 and Al_2O_3 phases were detected, local EDS analysis revealed an atomic ratio corresponding to the compound Al_2CO. It is known that this compound may act as an intermediate phase in the Al_4C_3–Al_2O_3 phase diagram [29].

It is likely that the molten aluminum, having filled a relatively large open pore (capillary), continued to penetrate into narrower capillaries between TiC particles, infiltrating the internal structure of the ceramic region with partial dissolution of TiC and subsequent formation of $TiAl_3$. The presence of a significant amount of aluminum carbide (and oxycarbide) in the large open pore is attributed to the fact that the excess graphite, remaining after the formation of the TiC SHS frame-
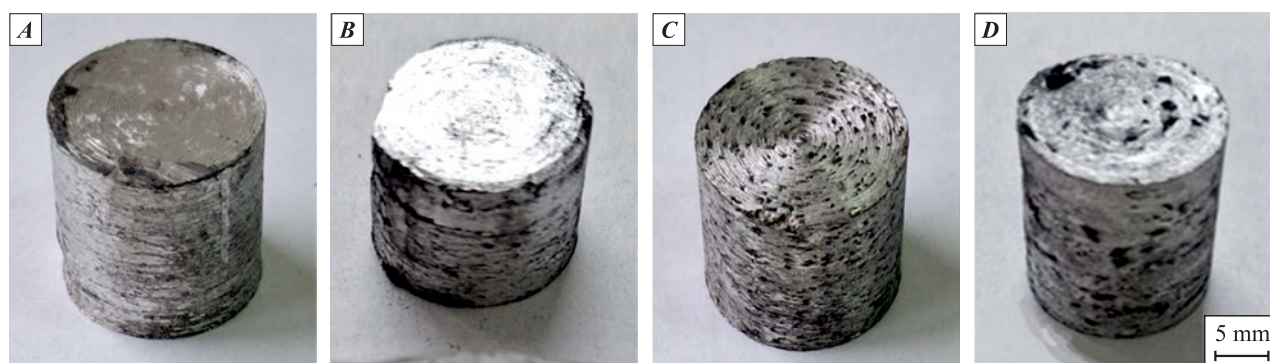

Fig. 2. External appearance of TiC–Al (*A*), TiC–C(S-2)–Al (*B*), TiC–C(GMZ)–Al (*C*), TiC–C(CF)–Al (*D*) composites

Рис. 2. Внешний вид композитов TiC–Al (*A*), TiC–C(С-2)–Al (*B*), TiC–C(ГМЗ)–Al (*C*) и TiC–C(УВ)–Al (*D*)
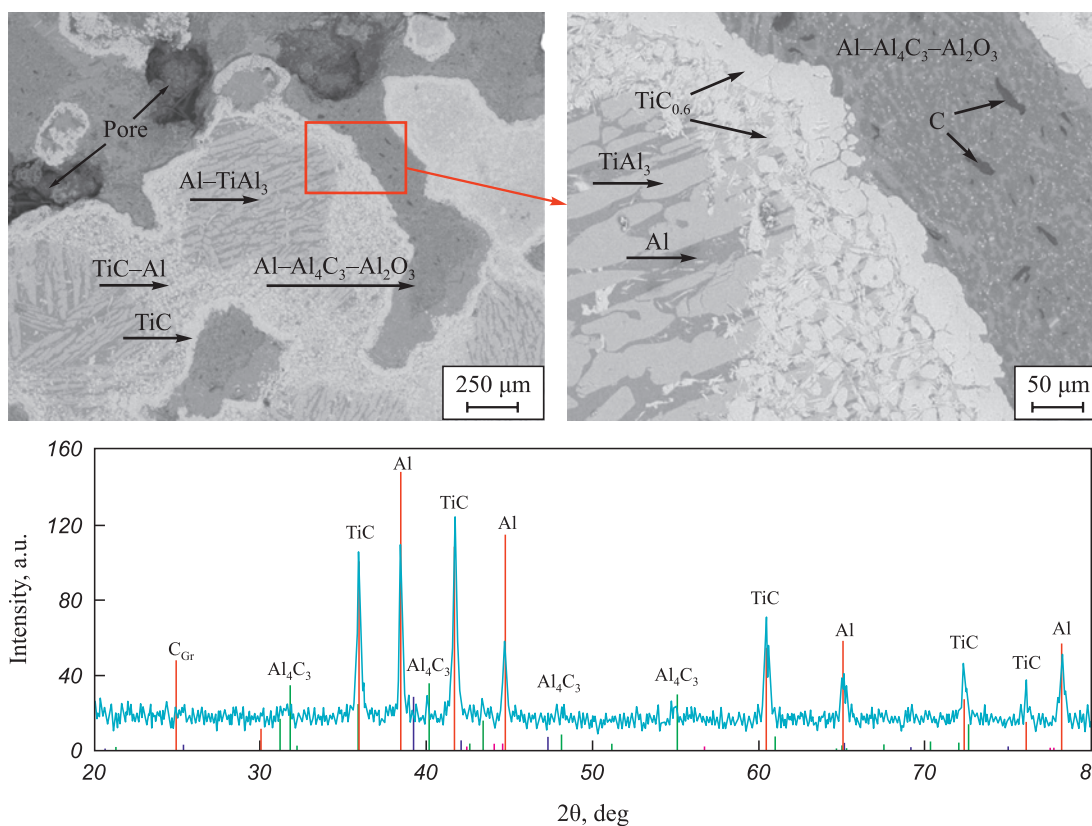
Fig. 3. Microstructure (top) and *X*-ray diffraction pattern (bottom) of the TiC–C(15 µm)–Al composite

Рис. 3. Микроструктура (сверху) и рентгеновская дифрактограмма (снизу) композита TiC–C(15 мкм)–Al

work, was concentrated in open pores and channels, which were subsequently filled with molten aluminum. In addition, isolated graphite particles measuring 15–30 µm were found within the Al matrix. The XRD pattern in Fig. 3 confirms the presence of the aforementioned phases; however, the peaks corresponding to $TiAl_3$, Al_2O_3, and graphite are within the background noise, indicating their low content in the composite.

Thus, graphite particles sized 10–15 µm almost completely dissolved in the molten aluminum, forming the secondary phase Al_4C_3. The formation of Al_4C_3 and $TiAl_3$ secondary phases in the TiC–Al system contributes to effective reactive wetting and strong adhesion between the metal and ceramic phases, which typically ensures high mechanical properties of the composite material [15]. According to the results of quantitative phase analysis, the phase composition of this composite is approximately as follows: 45–55 % Al, 35–40 % TiC, and up to 15 % secondary phases (Al_4C_3, $TiAl_3$, Al_2O_3). These values are approximate, since the XRD-based evaluation method has an error margin of up to 20 %, and the composite exhibits structural heterogeneity resulting from powder charge filling into the cylindrical crucible and the intense combustion process. The porosity of the TiC–C(S-2)–Al composite is approximately 7 %, and its average density is 3.11 g/cm³.

The microstructure and XRD pattern of the TiC–C(GMZ)–Al composite, fabricated using GMZ graphite with a particle size of 100–1000 µm, are shown in Fig. 4. Three regions with distinct colors and structural features are clearly visible. The most extensive area, appearing gray, corresponds to the aluminum matrix, within which large black regions (graphite), clusters of fine white particles (TiC), and a few elongated acicular gray particles were observed. These were identified as Al_2CO or a mixture of Al_4C_3 and Al_2O_3. The main differences compared to the composite prepared with fine graphite are the presence of large free graphite particles and a lower content of interfacial reaction products ($TiAl_3$, Al_4C_3, and Al_2O_3). In addition, the observed $TiC_{0.9}$ phase contains more carbon, with a composition close to the stoichiometric TiC.

The XRD pattern in Fig. 4 confirms the phase composition observed in the microstructure and identified by EDS analysis. A noticeable increase in the intensity of the free graphite peak compared to the data in Fig. 3 clearly indicates the retention of large graphite particles in the Al matrix, in contrast to the fine graphite particles, which almost completely dissolve in molten aluminum during composite fabrication. Quantitative phase analysis shows the following approximate composition of the obtained composite: 40–45 % Al,
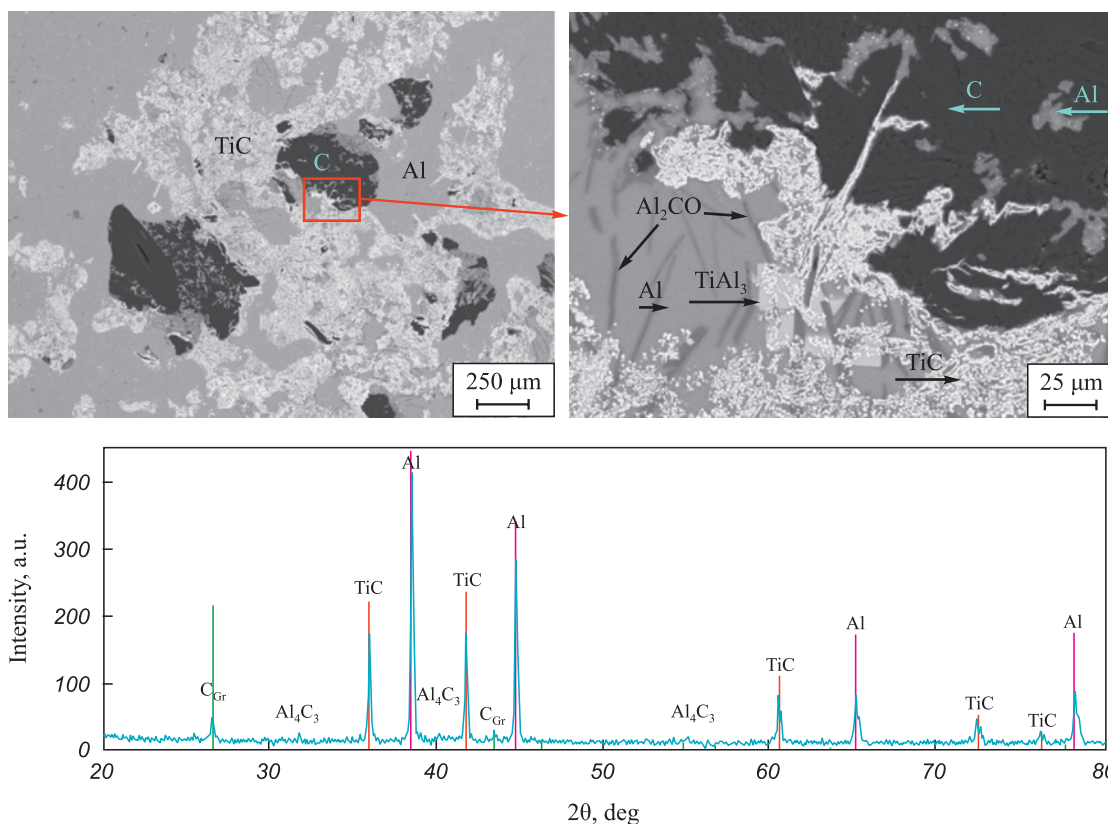
Fig. 4. Microstructure (top) and *X*-ray diffraction pattern (bottom) of the TiC–C(100–1000 μm)–Al composite

Рис. 4. Микроструктура (сверху) и рентгеновская дифрактограмма (снизу) композита TiC–C(100–1000 мкм)–Al

30–40 % TiC, 3–4 % graphite, and up to 15 % secondary phases (Al_4C_3, $TiAl_3$, Al_2O_3). The average porosity of the TiC–C(GMZ)–Al composite was 3.4 %, and its average density was 2.99 g/cm³.

The microstructure and *X*-ray diffraction pattern of the TiC–C(CF)–Al composite, fabricated with the addition of carbon fiber, are shown in Fig. 5. The gray aluminum matrix contains regions consisting of clusters of equiaxed TiC particles and black carbon fibers. Due to their different spatial orientations, the carbon fibers appear in either longitudinal or cross-section views. In the longitudinal view, ring-like structures approximately 10 μm in diameter are observed around the fibers, consisting of fine TiC particles less than 2 μm in size. These particles are presumed to form via a different mechanism, possibly related to the interaction between Al_4C_3 and $TiAl_3$ in the aluminum melt within a specific temperature range during cooling of the composite [15]. Outside the ring-shaped TiC particle zones, virtually no titanium carbide particles are observed in the aluminum matrix. Partial dissolution of carbon fibers in molten aluminum is indicated by a reduction in their diameter from the original 7 μm to 3–5 μm and the presence of Al_4C_3 around the fibers within the TiC rings. The XRD pattern confirms the presence of the main phases – Al, TiC, and, to a lesser extent,

Al_4C_3. Free graphite was not detected, as the carbon fibers preserved in the composite have an amorphous structure that is not detectable by XRD. According to the results of quantitative analysis, the approximate phase composition of the material is: 70–75 % Al, 15–20 % TiC, up to 3 % CF, and up to 15 % secondary phases (Al_4C_3, $TiAl_3$, Al_2O_3). The increased aluminum content and reduced TiC content are explained by the fact that when titanium and graphite powders are mixed with carbon fibers, the fibers tend to separate into thinner individual filaments, which greatly increases the total volume of the powder charge. As a result, after SHS, a TiC–CF framework is formed with greater porosity, allowing infiltration by a larger volume of molten aluminum compared to the TiC – graphite frameworks. Consequently, the average porosity of the final TiC–C(CF)–Al composite was only 1.9 %, the lowest among all samples, as was its average density, which was 2.74 g/cm³. The synthesis and structural features of porous TiC–CF SHS-based composite materials represent a separate subject requiring further investigation.

Due to the relatively high content of undesirable aluminum carbide (Al_4C_3) in the TiC–C(C-2)–Al composite fabricated with an excess of fine (15 μm) graphite powder grade C-2, its mechanical and tribologi-
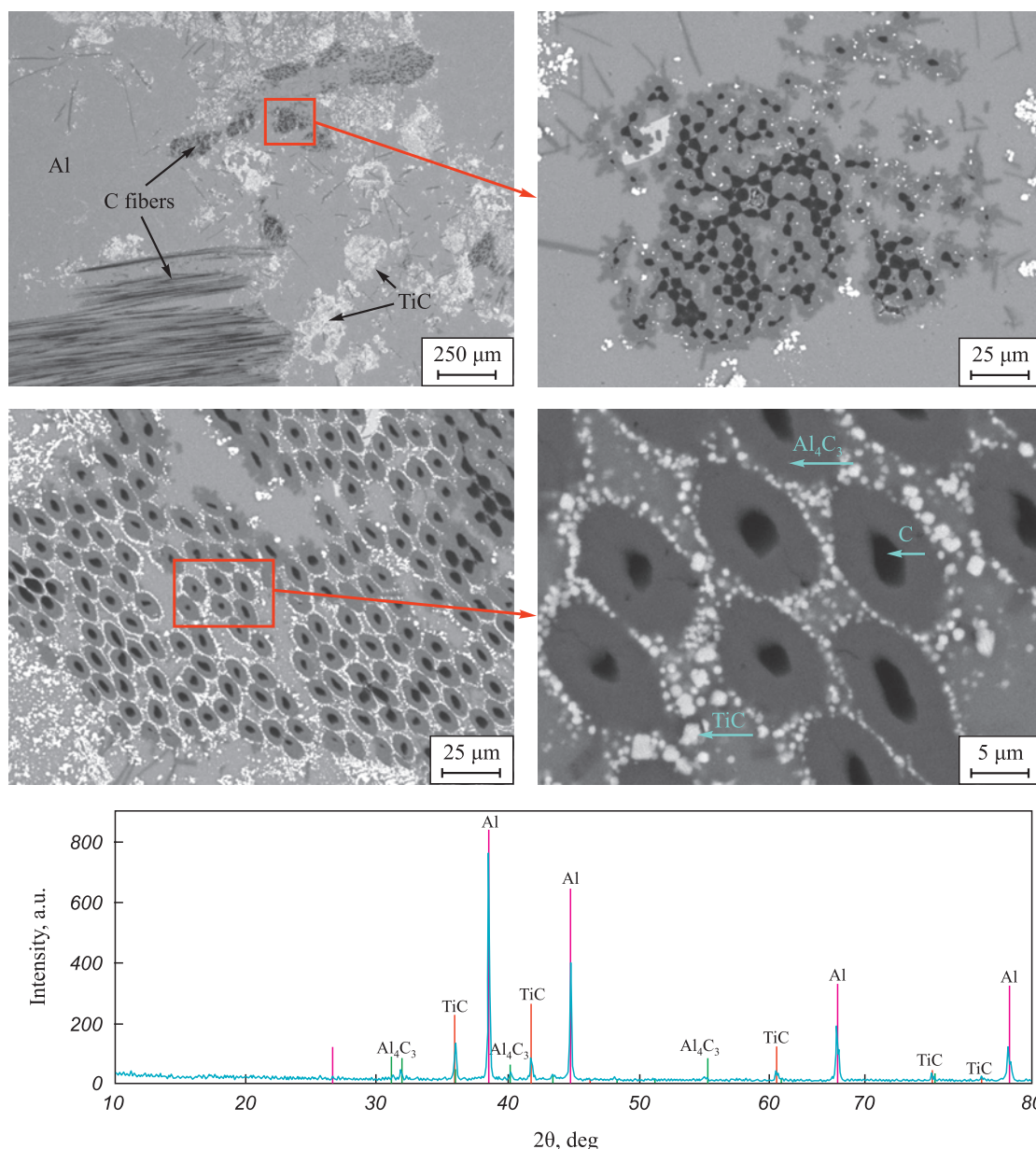
Fig. 5. Microstructure (top) and *X*-ray diffraction pattern (bottom) of the TiC–C(CF)–Al composite

Рис. 5. Микроструктура (сверху) и рентгеновская дифрактограмма (снизу) композита TiC–C(УВ)–Al

cal properties were not investigated. Al_4C_3 reacts with water to form Al_2O_3 and CH_4, making such composites phase- and structurally unstable not only in water but also in humid environments.

The results of density, hardness, and compressive property evaluation for the remaining samples of the studied TiC–Al and TiC–C–Al composite systems are presented in Table 1. As an example, Fig. 6 shows the compressive loading curves for each sample, reflecting the average result obtained from a series of tests on two samples. It can be seen that the TiC–C(100–1000 µm)–Al composite is brittle, while the other composites inherit the properties of the matrix and remain ductile.

The results obtained from the tribological tests are summarized in Table 2, while the general appearance of wear damage on the composite samples and indenters is shown in Fig. 7. The reported test results represent the arithmetic mean and standard deviation of the measured parameters, calculated from three identical tests conducted for each material.

Microscopic analysis of wear damage showed that the wear of the indenters is predominantly of abrasive origin, as evidenced by scratch marks aligned with the sliding direction (see central insets in Fig. 7, *a–c*). On the wear tracks of the tested composite samples, both scratches and signs of adhesive interaction between the contact surfaces are observed. Based on

PM & FC

POWDER METALLURGY AND FUNCTIONAL COATINGS. 2025;19(2):24–38
Umerov E.R., Amosov A.P., and etc. Structural, mechanical, and tribological properties of TiC–C–Al ...

Table 1. **Basic physical and mechanical properties of SHS-fabricated composites**

Таблица 1. **Основные физико-механические характеристики СВС-композитов**

Parameter	TiC–Al	TiC–C(100–1000 μm)–Al	TiC–C(CF)–Al
Density, g/cm^3	3.12 ± 0.01	2.99 ± 0.04	2.74 ± 0.09
Porosity, %	6.6	3.4	1.9
Hardness, HB	66.1 ± 3.9	59.9 ± 3.0	49.3 ± 9.4
Slope of the linear section of the $\sigma^c = f(\varepsilon)$ curve ($\mathrm{tg}^c\alpha$)	269.5 ± 19.1	173.5 ± 77.1	60.5 ± 41.7
Conventional compressive yield strength ($\sigma^c_{0.2}$), MPa	131.5 ± 16.3	135.5 ± 7.8	82.0 ± 9.9
Compressive strength (σ^{c*}_u), MPa	233.5 ± 13.4	203.5 ± 2.1	221.1 ± 18.4

Table 2. **Results of tribological testing of SHS-fabricated composites**

Таблица 2. **Результаты трибологических исследований СВС-композитов**

Parameter[*]	TiC–Al	TiC–C(100–1000 μm)–Al	TiC–C(CF)–Al
Tested materials			
S, mm	1.308 ± 0.174	1.033 ± 0.219	1.246 ± 0.109
h, μm	49.742 ± 23.490	26.240 ± 5.368	48.543 ± 16.453
V, mm^3	0.656 ± 0.300	0.221 ± 0.186	0.608 ± 0.319
$\dot{I}$, mm^3/min	$(9.889 \pm 4.527) \cdot 10^{-3}$	$(3.332 \pm 2.798) \cdot 10^{-3}$	$(9.156 \pm 0.005) \cdot 10^{-3}$
W, mm^{-2}	$(4.686 \pm 2.879) \cdot 10^5$	$(1.883 \pm 1.512) \cdot 10^6$	$(4.828 \pm 2.067) \cdot 10^5$
ε_I	1.0	3.0	1.1
Counterbody (spherical steel indenter)			
d, mm	1.516 ± 0.198	1.367 ± 0.051	1.386 ± 0.120
V, mm^3	0.045 ± 0.021	0.028 ± 0.004	0.030 ± 0.011
$\dot{I}$, mm^3/min	$(0.675 \pm 0.320) \cdot 10^{-3}$	$(0.417 \pm 0.064) \cdot 10^{-3}$	$(0.452 \pm 0.166) \cdot 10^{-3}$
W, mm^{-2}	$(6.774 \pm 3.871) \cdot 10^6$	$(9.176 \pm 1.318) \cdot 10^6$	$(8.997 \pm 2.746) \cdot 10^6$
ε_I	1.0	1.6	1.5
General characteristics of the friction pair			
μ_{max}	1.692 ± 0.214	1.639 ± 0.222	1.781 ± 0.111
μ_{av}	0.881 ± 0.041	0.982 ± 0.076	0.919 ± 0.177
α	0.5	0.6	0.5

[*]S and h – average wear track width and depth; V – volumetric wear; $\dot{I}$ – wear rate; W – wear resistance; ε_I – relative wear resistance; μ_{av} and μ_{max} – average and maximum kinetic coefficient of friction; α – friction coefficient stability.

the above observations, it can be concluded that in the friction pair 100Cr6/TiC–C–Al (with carbon additive content C ≥ 0), adhesion is promoted by the soft aluminum matrix, which occupies the larger volume fraction in the composite and has the lowest melting point. The hard refractory particles TiC, Al_2O_3, Al_2CO, $TiAl_3$, and Al_4C_3 suppress adhesion but act as sources of abrasive damage to the contact surfaces. Logically, the abrasive effect is caused by both the particles embedded in the composite structure and those released into the wear debris in free form.

Another component of the wear debris consists of particles originating from the steel ball indenter. On the one hand, these particles serve as abrasives; on the other, like the Al matrix, they contribute to adhesion between the sample and the indenter. Nevertheless, under the tested conditions, the predominant wear mechanism should be considered abrasive wear. This conclusion is supported by the observation that during sliding, wear debris becomes embedded in the soft matrix, gradually altering the surface composition of the composites by increasing the proportion of hard
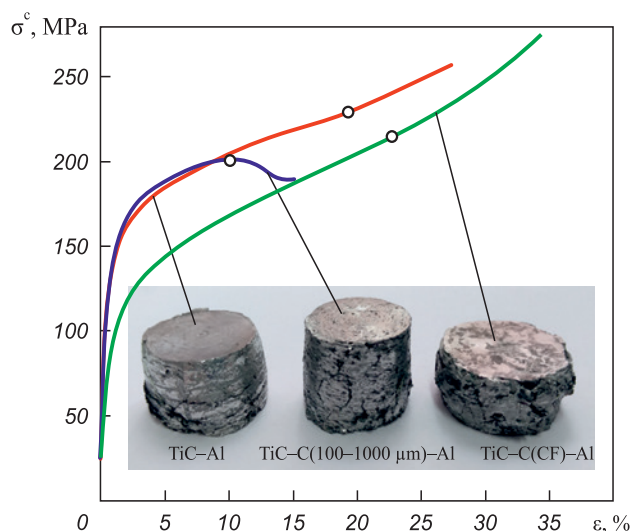
Fig. 6. General appearance of the composite samples after compression testing and the corresponding stress–strain curves
Asterisks indicate the values of σ_u^{c*}

Рис. 6. Общий вид образцов композитов после испытаний на сжатие и соответствующие кривые нагружения
Точками отмечены значения σ_u^{c*}

gradually decrease. Verification of this hypothesis would require the use of precision methods to monitor wear kinetics and related effects during testing, which is the subject of future dedicated tribological studies. Within the scope of the present work, the following conclusions can be drawn.

The presence of graphite in the TiC–C–Al composite increased the average coefficient of friction but reduced its maximum value as well as all wear-related parameters (see Table 2), especially in the case of coarse graphite (100–1000 μm) addition, where the lowest wear was recorded for both the composite and the indenter, along with the highest friction stability (α). According to the relative wear resistance parameter (ε_l), the addition of carbon resulted in a clear reduction in wear of both the TiC–C(100–1000 μm)–Al and TiC–C(CF)–Al composites compared to the baseline TiC–Al composite. A sharp increase in indenter wear resistance was also observed for TiC–C(100–1000 μm)–Al, while the improvement was less pronounced for TiC–C(CF)–Al.

Profilometric analysis revealed that in the 100Cr6/TiC–Al pair, mutual abrasive wear of both the ball and the sample occurs, resulting in a wear track cross-section close to a circular shape along the entire depth of wear (see Fig. 7, *d* and Table 2). In the 100Cr6/TiC–C(100–1000 μm)–Al pair, the predominant wear occurs on the ball, as the sample shows
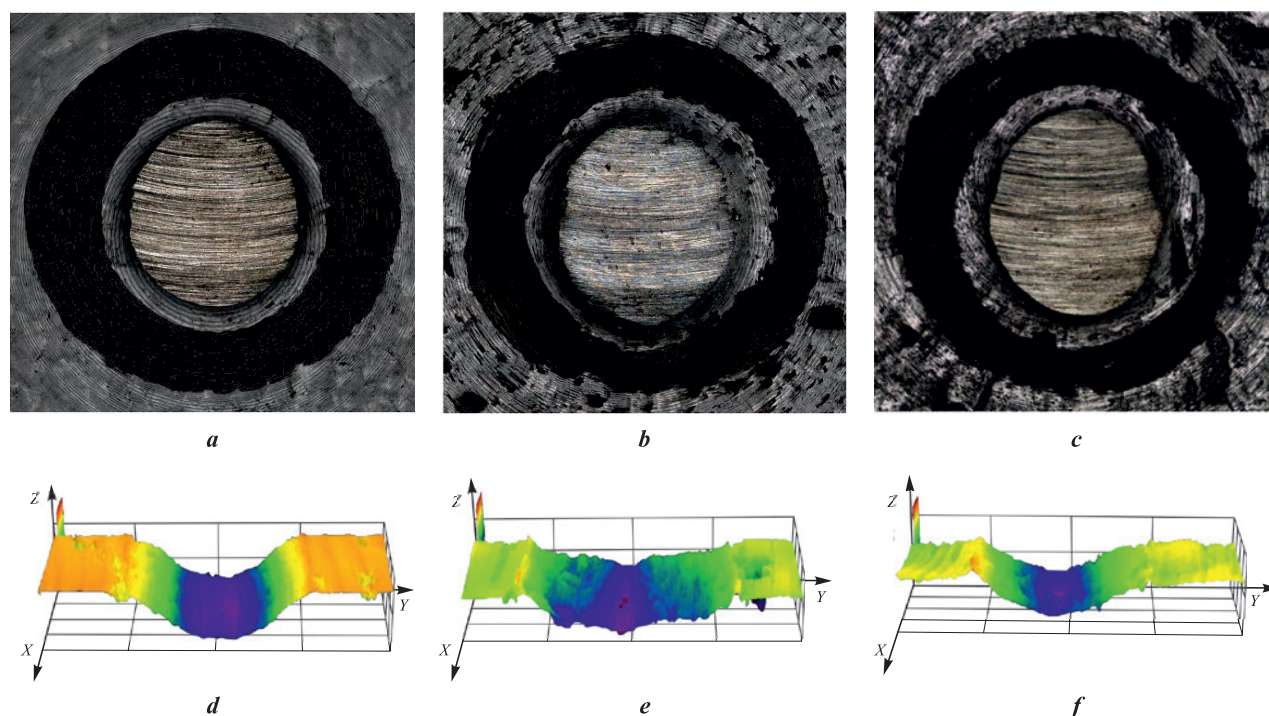
particles. This explains the purely abrasive wear observed on the indenter. According to the hypothesis proposed in [30], at C = 0 the instantaneous wear rate should reach a constant value, while at C > 0 it should

Fig. 7. General view of wear damage on composite samples and indenters (*a–c*), and 3D cross-sectional profiles of wear tracks (*d–f*)
a, *d* – TiC–Al; *b*, *e* – TiC–C(100–1000 μm)–Al; *c*, *f* – TiC–C(CF)–Al

Рис. 7. Общий вид повреждений образцов и инденторов (*a–c*), а также 3D-профиль сечения дорожек трения (*d–f*)
a, *d* – TiC–Al; *b*, *e* – TiC–C(100–1000 мкм)–Al; *c*, *f* – TiC–C(УВ)–Al

PM & FC

POWDER METALLURGY AND FUNCTIONAL COATINGS. 2025;19(2):24–38

Umerov E.R., Amosov A.P., and etc. Structural, mechanical, and tribological properties of TiC–C–Al ...

more uniform wear over the contact area with only slight penetration (Fig. 7, *e*, Table 2). The wear mode in the 100Cr6/TiC–C(CF)–Al pair is intermediate – it penetrates deeper but forms a cross-sectional profile resembling a triangle (Fig. 7, *f*, Table 2). This supports the idea that carbon fiber begins to function as a lubricant at a certain point in the test, once the contact pressure decreases due to wear and sufficient amounts of CF-containing debris accumulate on the friction surface to provide lubrication.

As also shown in Table 2, the studied materials consistently fall into wear resistance class 5 ($W \sim 10^5 \div 10^6$ mm^{-2}), while the steel counterbody corresponds to class 6 ($W \sim 10^6 \div 10^7$ mm^{-2}). The addition of coarse graphite (100–1000 µm) increases the class rating to 6 and 7, respectively. Considering that sliding bearings typically use materials of wear resistance classes 5–8 [31], the studied composites are promising for such applications, even under dry friction conditions. It is known that the service life of a tribological assembly can be significantly extended in the presence of a liquid lubricant. In this regard, the porosity of SHS-fabricated TiC–C–Al composites may play a beneficial role by enabling oil impregnation and operation in a lubricated environment. However, such operating conditions and wear modes require further experimental studies and will be the subject of future research.

The standard deviations of the wear evaluation parameters (see Table 2) indicate a wide scatter in the tribological test results, which, as noted earlier, can be attributed to the inhomogeneous distribution of TiC and C particles in the Al matrix and the inherent porosity of the composite materials. This leads to high friction coefficients and uneven wear track widths and depths (see Table 2 and Fig. 7). Nonetheless, it is worth noting that the addition of coarse graphite (100–1000 µm), even under these structurally inhomogeneous conditions, improves the frictional stability.

Conclusions

1. The feasibility of fabricating hybrid composites of the TiC–C–Al system was examined by combining SHS for the synthesis of a porous TiC–C ceramic–carbon framework with subsequent spontaneous infiltration using molten aluminum. Three types of composites were produced with 100 % excess carbon – relative to the carbon mass in the stoichiometric Ti + C mixture – added to the initial powder charge in the form of fine and coarse graphite powders and chopped carbon fiber: TiC–C(15 µm)–Al, TiC–C(100–1000 µm)–Al, and TiC–C(CF)–Al. For comparison, a TiC–Al composite without excess carbon was also fabricated.

2. The reactive nature of TiC and C wetting by molten aluminum was confirmed by the increased content of secondary interfacial reaction products such as Al_4C_3, $TiAl_3$, Al_2O_3, and possibly Al_2CO. Their total content reached up to 15 % in all three composites synthesized with excess carbon, while in the sample without such additives it did not exceed 5 %.

3. The use of excess fine graphite (15 µm, grade C-2) in the charge leads to its almost complete dissolution in molten Al and its absence in the final composite. The use of coarse graphite (100–1000 µm) significantly reduces interfacial interaction and largely preserves it in the form of free graphite in the resulting composite (up to 3–4 %). Carbon fiber demonstrates intermediate stability in molten Al compared to fine and coarse graphite powders, with up to 3 % of free carbon retained in the composite in the form of amorphous carbon fibers.

4. The ratio of TiC–C ceramic to Al metal content in the hybrid composites and their residual porosity significantly depend on the type of excess carbon additive (graphite or carbon fiber). The TiC phase concentration is highest in the TiC–Al composite without excess carbon (50–55 %), as is the porosity, which can reach up to 8 %. When excess carbon is introduced, the TiC content and porosity decrease to 35–40 % and 7 %, respectively, in the case of fine graphite (C-2); to 30–40 % and 3.4 % with coarse graphite (GMZ); and to 15–20 % and 1.9 % when carbon fiber is used. In the latter case, the Al phase content reaches its maximum value of 70–75 %.

5. The compressive strength of the Al-matrix composites TiC–Al, TiC–C(100–1000 µm)–Al, and TiC–C(CF)–Al was 233.5, 203.5, and 221.1 MPa, respectively, while the conventional compressive yield strength was 131.5, 135.5, and 82.0 MPa, respectively. Thus, the introduction of excess carbon and its presence in the final composite reduce the strength of the hybrid composites compared to the TiC–Al sample without carbon addition. At the same time, the TiC–C(100–1000 µm)–Al composite exhibits brittle behavior, whereas the other composites inherit the properties of the matrix and remain sufficiently ductile.

6. During friction and wear of the investigated TiC–C–Al hybrid composites in contact with a steel counterbody, abrasive wear was found to be the dominant mechanism, accompanied by a high coefficient of friction (0.88–0.98). Under these conditions, the TiC–C(100–1000 µm)–Al composite demonstrated the best tribological performance, with three times lower wear, which is attributed to the presence of self-lubricating properties retained from the beginning of the friction and wear process. It was shown that all the studied variants of hybrid composites are promis-

ing for use in sliding bearing applications. Moreover, their porosity, despite its observed negative effect on the stability of friction and wear behavior, may potentially be advantageous for lubricant impregnation in future applications.

7. Further research is planned to focus on identifying Al-based matrix alloys for tribological applications that exhibit lower chemical reactivity toward graphite during infiltration, which would enable further improvement of the tribological performance of TiC – graphite – Al(alloy) composites. It is also necessary to study in more detail the kinetics of wear accumulation, variations in the coefficient of friction, and related effects (e.g., acoustic emission) during the friction and wear of TiC–C–Al hybrid composites under dry and boundary lubrication conditions, including after lubricant impregnation and immersion in a liquid lubrication medium.

References / Список литературы

1. Rohatgi P.K., Tabandeh-Khorshid M., Omrani E., Lovell M.R., Menezes P.L. Tribology of metal matrix composites. In: *Tribology for Scientists and Engineers*. NY: Springer, 2013. P. 233–268.
   https://doi.org/10.1007/978-1-4614-1945-7_8

2. Ayar M.S., George P.M., Patel R.R. Advanced research progresses in aluminium metal matrix composites: An overview. In: *Proceedings of the 14th Asia-Pacific physics conference*. AIP Publishing, 2021. No. 2317(1). P. 20–26. https://doi.org/10.1063/5.0036141

3. Kar A., Sharma A., Kumar S. A critical review on recent advancements in aluminium-based metal matrix composites. *Crystals (Basel)*. 2024;14(5):412.
   https://doi.org/10.3390/cryst14050412

4. Ajay K.P., Rohatgi P., Weiss D. 50 Years of foundry-produced metal matrix composites and future opportunities. *International Journal of Metalcasting*. 2020;14(2):291–317.
   https://doi.org/10.1007/s40962-019-00375-4

5. Kostikov V. Composite materials based on aluminum alloys reinforced with carbon fibers. Moscow: Intermet Engineering, 2000. 445 p. (In Russ.).

   Костиков В. Композиционные материалы на основе алюминиевых сплавов, армированных углеродными волокнами. М.: Интермет Инжиниринг, 2000. 445 с.

6. Singh N., Belokar R.M., Walia R.S. A critical review on advanced reinforcements and base materials on hybrid metal matrix composites. *Silicon*. 2022;14(2):1–24.
   https://doi.org/10.1007/s12633-020-00853-z

7. Arunkumar S., Guhan R., Srivathsan A., Rithik A. Fabrication methods of aluminium metal matrix composite: A state of review. *International Research Journal on Advanced Engineering and Management (IRJAEM)*. 2024;2(03):528–537.
   https://doi.org/10.47392/irjaem.2024.0073

8. Rogachev A.S., Mukasyan A.S. Combustion for material synthesis. New York: CRC Press, 2014. 424 p.
   https://doi.org/10.1201/b17842

9. Borovinskaya I., Gromov A., Levashov E., Maksimov Y., Mukasyan A., Rogachev A. Concise encyclopedia of self-propagating high-temperature synthesis: History, theory, technology, and products. Elsevier, 2017. 432 p.

10. Kaya M., Orhan N., Tosun G. The effect of the combustion channels on the compressive strength of porous NiTi shape memory alloy fabricated by SHS as implant material. *Current Opinion in Solid State and Materials Science*. 2010;14(1):21–25.
    https://doi.org/10.1016/j.cossms.2009.07.002

11. Rohatgi P.K., Gupta N., Alaraj S. Thermal expansion of aluminum–fly ash cenosphere composites synthesized by pressure infiltration technique. *Journal of Composite Materials*. 2006;40(13):1163–1174.
    https://doi.org/10.1177/0021998305057379

12. Zhou S.M., Zhang X.B, Ding Z.P., Min C.Y., Xu G.L., Zhu W.M. Fabrication and tribological properties of carbon nanotubes reinforced Al composites prepared by pressureless infiltration technique. *Composites. Part A: Applied Science and Manufacturing*. 2007;38(2):301–306.
    https://doi.org/10.1016/j.compositesa.2006.04.004

13. Gulevsky V.A., Miroshkin N.Yu., Tsurikhin S.N., Gundrov O.Yu. More details about impregnation of carbon graphite with aluminum. *Izvestiya Volgogradskogo gosudarstvennogo tekhnicheskogo universiteta*. 2020;(7(242)):77–82. (In Russ.).
    https://doi.org/10.35211/1990-5297-2020-7-242-77-82

    Гулевский В.А., Мирошкин Н.Ю., Цурихин С.Н., Гундров О.Ю. Подробнее о пропитке углеграфита алюминием. *Известия Волгоградского государственного технического университета*. 2020;7(242):77–82.
    https://doi.org/10.35211/1990-5297-2020-7-242-77-82

14. Lee M., Choi Y., Sugio K., Matsugi K., Sasaki G. Effect of aluminum carbide on thermal conductivity of the unidirectional CF/Al composites fabricated by low pressure infiltration process. *Composites Science and Technology*. 2014;97:1–5.
    https://doi.org/10.1016/j.compscitech.2014.03.022

15. Contreras Cuevas A., Bedolla Becerril E., Martínez M.S, Lemus Ruiz J. Fabrication processes for metal matrix composites. In: *Metal Matrix Composites: Wetting and Infiltration*. Cham: Springer Nature Switzerland AG, 2018. P. 83–114. https://doi.org/10.1007/978-3-319-91854-9_3

16. Mikheev R.S. Promising coatings with enhanced tribotechnical properties made of composite materials based on non-ferrous metals: Abstract of the dissertation of Dr. Sci.(Eng.). Moscow: Institute of Metallurgy and Materials Science named after A. A. Baykov, 2018. (In Russ.).

    Михеев Р.С. Перспективные покрытия с повышенными триботехническими свойствами из композиционных материалов на основе цветных металлов: Автореф. дис.… д.т.н. М.: Институт металлургии и материаловедения им. А.А. Байкова, 2018.

17. Riahi A.R., Alpas A.T. The role of tribo-layers on the sliding wear behavior of graphitic aluminum matrix composites. *Wear*. 2001;1(1-12):1396–1407.
    https://doi.org/10.1016/S0043-1648(01)00796-7

18. Ravindran P., Manisekar K., Narayanasamy R., Narayanasamy P. Tribological behaviour of powder metallurgy-

processed aluminium hybrid composites with the addition of graphite solid lubricant. *Ceramics International.* 2013;39(2):1169–82.
https://doi.org/10.1016/j.ceramint.2012.07.041

19. Baradeswaran A., Perumal A.E. Wear and mechanical characteristics of Al 7075/graphite composites. *Composites. Part B: Engineering.* 2014;56:472–476.
https://doi.org/10.1016/j.compositesb.2013.08.073

20. Scaria C.T., Pugazhenthi R., Daniel A.A., Santhosh K. Mechanical and wear studies on AA7075/nano TiC/graphite hybrid composites for tribological applications. *Advances in Materials Science and Engineering.* 2022;(1):1–8.
https://doi.org/10.1155/2022/5320363

21. Fallahdoost H., Nouri A., Azimi A. Dual functions of TiC nanoparticles on tribological performance of Al/graphite composites. *Journal of Physics and Chemistry of Solids.* 2016;93:137–144.
https://doi.org/10.1016/j.jpcs.2016.02.020

22. Umerov E.R., Latukhin E.I., Amosov A.P., Kichaev P.E. Preparation of Ti₃SiC₂–Sn(Pb) cermet by SHS of Ti₃SiC₂ porous skeleton with subsequent spontaneous infiltration with Sn–Pb melt. *International Journal of Self-Propagating High-Temperature Synthesis.* 2023;32(1):30–35.
https://doi.org/10.3103/S1061386223010089

23. Latukhin E.I., Umerov E.R., Amosov A.P. Preparation of Ti₃AlC₂–Al cermets by combined use of SHS of Ti₃AlC₂ porous skeleton and spontaneous infiltration with Al and Al-based melts. *International Journal of Self-Propagating High-Temperature Synthesis.* 2023;32(1):23–29.
https://doi.org/10.3103/S1061386223010041

24. Amosov A.P., Latukhin E.I., Umerov E.R. Applying infiltration processes and self-propagating high-temperature synthesis for manufacturing cermets: A review. *Russian Journal of Non-Ferrous Metals.* 2022;63(1):81–100.
https://doi.org/10.3103/S1067821222010047

Амосов А.П., Латухин Е.И., Умеров Э.Р. Применение процессов инфильтрации и самораспространяющегося высокотемпературного синтеза для получения керметов: Обзор. *Известия вузов. Цветная металлургия.* 2021;27(6):52–75.
https://doi.org/10.17073/0021-3438-2021-6-52-75

25. Davydov D.M., Amosov A.P., Latukhin E.I., Umerov E.R., Novikov V.A. Features of the composition and microstructure of porous skeletons of MAX-phases Ti₃AlC₂ and Ti₃SiC₂ produced by the SHS method in air and in a protective shell of sand. *Vestnik Sibirskogo gosudarstvennogo industrial'nogo universiteta.* 2023;(4):88–97. (In Russ.).
https://doi.org/10.57070/2304-4497-2023-4(46)-88-97

Давыдов Д.М., Амосов А.П., Латухин Е.И., Умеров Э.Р., Новиков В.А.. особенности состава и микроструктуры пористых каркасов МАХ-фаз Ti₃AlC₂ и Ti₃SiC₂, получаемых методом СВС на воздухе и в защитной оболочке из песка. *Вестник Сибирского государственного индустриального университета.* 2023;4:88–97.
https://doi.org/10.57070/2304-4497-2023-4(46)-88-97

26. Davydov D.M., Umerov E.R., Amosov A.P., Latukhin E.I. Influence of starting reagents on the formation of Ti₃SiC₂ porous skeleton by SHS in air. *International Journal of Self-Propagating High-Temperature Synthesis.* 2024;33(1):26–32.
https://doi.org/10.3103/S1061386224010023

27. Amosov A., Amosov E., Latukhin E., Kichaev P., Umerov E. Producing TiC–Al cermet by combustion synthesis of TiC porous skeleton with spontaneous infiltration by aluminum melt. In: *Proc. 2020 7ᵗʰ International Congress on Energy Fluxes and Radiation Effects. IEEE.* 2020. P. 1057–1062.
https://doi.org/10.1109/EFRE47760.2020.9241903

28. Umerov E.R. Manufacturing cermets using self-propagating high-temperature synthesis of ceramic skeletons TiC, Ti₃SiC₂, Ti₃AlC₂ and subsequent spontaneous infiltration with melts of metals Al, Sn, Cu: Abstract of the Dissertation of Cand. Sci.(Eng.). Samara: SamSTU, 2023. (In Russ.).

Умеров Э.Р. Получение керметов с использованием самораспространяющегося высокотемпературного синтеза керамических каркасов TiC, Ti₃SiC₂, Ti₃AlC₂ и последующей самопроизвольной инфильтрации расплавами металлов Al, Sn, Cu: Автореф. дис.… к.т.н. Самара: СамГТУ, 2023.

29. Foster L.M., Long G., Hunter M.S. Reactions between aluminum oxide and carbon the Al₂O₃–Al₄C₃ phase diagram. *Journal of the American Ceramic Society.* 1956;39(1):1–11.
https://doi.org/10.1111/j.1151-2916.1956.tb15588.x

30. Umerov E., Amosov A., Latukhin E., Kiran K.U., Choi H., Saha S., Roy S. Fabrication of MAX-phase composites by novel combustion synthesis and spontaneous metal melt infiltration: Structure and tribological behaviors. *Advanced Engineering Materials.* 2024;26(8):2301792. https://doi.org/10.1002/adem.202301792

31. Chichinadze A., Berliner E., Braun E., Bushe N., Buyanovsky I., Hecker F. Friction, wear and lubrication (tribology and tribotechnics). Moscow: Mashinostroenie, 2003. 575 p. (In Russ.).

Чичинадзе А., Берлинер Э., Браун Э., Буше Н., Буяновский И., Геккер Ф. Трение, износ и смазка (трибология и триботехника). М.: Машиностроение, 2003. 575 с.

Information about the Authors / Сведения об авторах

Emil R. Umerov – Cand. Sci. (Eng.), Leading Research Fellow of the Department of Metals Science, Powder Metallurgy, Nanomaterials, Samara State Technical University (SamSTU)
🆔 **ORCID**: 0000-0002-2050-6899
✉ **E-mail**: umeroff2017@yandex.ru

Эмиль Ринатович Умеров – к.т.н., вед. науч. сотрудник кафедры «Металловедение, порошковая металлургия, наноматериалы», Самарский государственный технический университет (СамГТУ)
🆔 **ORCID**: 0000-0002-2050-6899
✉ **E-mail**: umeroff2017@yandex.ru

ПМ и ФП
ИЗВЕСТИЯ ВУЗОВ

ИЗВЕСТИЯ ВУЗОВ. Порошковая металлургия и функциональные покрытия. 2025;19(2):24–38
Умеров Э.Р., Амосов А.П. и др. Структурные, механические и трибологические особенности гибридных ...

Aleksandr P. Amosov – Dr. Sci. (Phys.-Math.), Head of the Department of Metals Science, Powder Metallurgy, Nanomaterials, SamSTU
ORCID: 0000-0002-1510-6567
E-mail: egundor@yandex.ru

Evgeny I. Latukhin – Cand. Sci. (Eng.), Associate Professor of the Department of Metals Science, Powder Metallurgy, Nanomaterials, SamSTU
ORCID: 0000-0002-2071-3521
E-mail: evgelat@yandex.ru

Andrey D. Kachura – Postgraduate Student of the Department of Metals Science, Powder Metallurgy, Nanomaterials, SamSTU
ORCID: 0000-0001-9246-5638
E-mail: ruw223@mail.ru

Igor A. Rastegaev – Dr. Sci. (Eng.), Leading Researcher of the Magnesium Materials Design Laboratory, Togliatti State University (TSU)
ORCID: 0000-0003-3807-8105
E-mail: RastIgAev@yandex.ru

Maxim A. Afanasiev – Leading Engineer of the Magnesium Materials Design Laboratory, (TSU)
ORCID: 0000-0003-1424-7277
E-mail: maxwel-i@yandex.ru

Александр Петрович Амосов – д.ф.-м.н., зав. кафедрой «Металловедение, порошковая металлургия, наноматериалы», СамГТУ
ORCID: 0000-0002-1510-6567
E-mail: egundor@yandex.ru

Евгений Иванович Латухин – к.т.н., доцент кафедры «Металловедение, порошковая металлургия, наноматериалы», СамГТУ
ORCID: 0000-0002-2071-3521
E-mail: evgelat@yandex.ru

Андрей Дмитриевич Качура – аспирант кафедры «Металловедение, порошковая металлургия, наноматериалы», СамГТУ
ORCID: 0000-0001-9246-5638
E-mail: ruw223@mail.ru

Игорь Анатольевич Растегаев – д.т.н., вед. науч. сотрудник лаборатории дизайна магниевых материалов, Научно-исследовательский институт прогрессивных технологий, Тольяттинский государственный университет (ТГУ)
ORCID: 0000-0003-3807-8105
E-mail: RastIgAev@yandex.ru

Максим Анатольевич Афанасьев – вед. инженер лаборатории дизайна магниевых материалов, ТГУ
ORCID: 0000-0003-1424-7277
E-mail: maxwel-i@yandex.ru

Contribution of the Authors   *Вклад авторов*

E. R. Umerov – defined the purpose of the work, conducted experiments, wrote the article.
A. P. Amosov – defined the purpose of the work, participated in the discussion of the results, wrote the article.
E. I. Latukhin – conducted experiments, participated in the discussion of the results, wrote the article.
A. D. Kachura – prepared the charge mixtures and initial samples, participated in the discussion of the results.
I. A. Rastegaev – conducted tribological studies of the samples, participated in the discussion of the results.
M. A. Afanasiev – conducted studies of the mechanical properties of the samples, participated in the discussion of the results.

Э. Р. Умеров – определение цели работы, проведение экспериментов, написание текста статьи.
А. П. Амосов – определение цели работы, участие в обсуждении результатов, написание текста статьи.
Е. И. Латухин – проведение экспериментов, участие в обсуждении результатов.
А. Д. Качура – подготовка шихтовых смесей и исходных образцов, участие в обсуждении результатов.
И. А. Растегаев – проведение трибологических исследований образцов, участие в обсуждении результатов.
М. А. Афанасьев – проведение исследований механических свойств образцов, участие в обсуждении результатов.